Published in Physical Review Letters 42, issue 8, 5369-5372, 1990
which should be used for any reference to this work

Nondipole channels in the electron-energy-loss structure near the 3*s* edge of copper

P. Aebi,* M. Erbudak, F. Vanini,† D. D. Vvedensky,‡ and G. Kostorz
Institut für Angewandte Physik, Eidgenössische Technische Hochschule Zürich, CH-8093 Zürich, Switzerland

Electron transitions near the 3*s* edge of copper are investigated with electron-energy-loss spectroscopy and compared with real-space multiple-scattering calculations. Calculating the generalized oscillator strength illustrates the importance of dipole-forbidden transitions in the near-edge region and shows the feasibility of making detailed comparisons between theory and electron-energy-loss measurements without resorting to the dipole approximation.

There continues to be wide-ranging interest in probing unoccupied electronic states using electron and photon primary sources. Excitation of core electrons has, in particular, attracted considerable attention, leading to the development of techniques such as extended x-ray-absorption fine structure[1] and the electronic analogue, extended-energy-loss fine structure,[2] which are used for probing the local structure of the excited atom. Excitation of inner-shell electrons can also be used to investigate the role of the core-hole potential[3] in the excitation process and other more complex final-state effects, such as the influence of multiplet structure.[4] In all of these studies the calculation of the underlying single-particle excitation spectrum is of paramount importance either for the direct interpretation of the excitation spectrum, or for assessing the requirements of a more refined theory.

In this Rapid Communication we present measurements of the electron-energy-loss spectrum near the Cu 3*s* edge and accompanying calculations using a real-space multiple-scattering formalism that make no presumption concerning the validity of dipole selection rules. In fact, calculations of the generalized oscillator strength (GOS) show that different core edges behave quite differently with regard to dipole selection rules. Near some edges, the dipole-allowed transitions dominate even at large momentum transfer, while for others, dipole-forbidden transitions appear even at small momentum transfer. Our calculations are the first to show the feasibility of making detailed comparisons between theory and electron-energy-loss measurements including the multiple scattering of the ejected core electron and without resorting to the dipole approximation. This work thus extends the applicability of the approach used so successfully to calculate the near-edge x-ray-absorption fine structure[5,6] and complements the recent work using an analogous approach to calculate x-ray bremsstrahlung isochromat fine structure.[7,8] Furthermore, the approach presented here may be employed in more general theories that also incorporate the dynamical scattering of the transmitted fast electrons.[9]

The measurements were performed in an ultrahigh-vacuum (UHV) apparatus with a total pressure of 10^{-8} Pa range. A copper single-crystal surface was oriented with the x-ray Laue method and electropolished. The surface was cleaned in UHV by etching with Ar^+ and heated to 900 K until no traces of O, C, and Ar were detectable by Auger-electron spectroscopy. Surfaces so prepared delivered sharp low-energy electron diffraction (LEED) patterns. Spectra were recorded with a Riber Mac-2 energy analyzer operating with a constant energy resolution of 0.4 eV. Experimental details are described elsewhere.[10] The data acquisition time was several hours.

To calculate the transition probability per unit time, W, including the various excitation channels, we apply the Fermi "golden rule:"

$$W=\frac{2\pi}{\hbar}\sum_s |M_{E_s,p_s}^{E_{\rm inc},p_{\rm inc}}|^2\,\delta(E_{\rm inc}+E_i-E_f-E_s)\,, \qquad (1)$$

where the subscript "inc" denotes quantities for the initial state of the primary electron, i for the initial core state, f for the final state of the primary electron after inelastic scattering, and s for the scattering state of the photoelectron. Without allowing for exchange,[11,12] the matrix elements are given by

$$M_{E_s,p_s}^{E_{\rm inc},p_{\rm inc}}=\int d\mathbf{r}_1\int d\mathbf{r}_2\,\psi_i^*(\mathbf{r}_1)\psi_{\rm inc}^*(\mathbf{r}_2) \times V(\mathbf{r}_1,\mathbf{r}_2)\psi_f(\mathbf{r}_2)\psi_s(\mathbf{r}_1)\,, \qquad (2)$$

where $V(\mathbf{r}_1,\mathbf{r}_2)$ is an unscreened Coulomb potential, $V(\mathbf{r}_1,\mathbf{r}_2)=1/|\mathbf{r}_1-\mathbf{r}_2|$, and the charge e has been set to unity.

Taking plane waves for the initial and final states of the primary electron (the Born approximation), $\psi_{\rm inc}=\exp(i\mathbf{k}_{\rm inc}\cdot\mathbf{r})$, $\psi_f=\exp(i\mathbf{k}_f\cdot\mathbf{r})$, and writing (1) in the form

$$W=-\frac{2}{\hbar}{\rm Im}\langle i,{\rm inc}|VG^+V|f,s\rangle\,, \qquad (3)$$

where G^+ is the Green's function (at energy E) of the scattering photoelectron, the transition rate for momentum transfer $\mathbf{q}=\mathbf{k}_f-\mathbf{k}_{\rm inc}$ of the primary beam can be written as[5,6]

$$W=\frac{32\pi^2}{\hbar q^4}k\left(\sum_L |M_{i,L}|^2-{\rm Im}\sum_{L,L'}M_{i,L}\frac{\tau_{LL'}^{00}(E_s)-it_l^0(E_s)\delta_{l,l'}}{\sin[\delta_l(E_s)]\sin[\delta_{l'}(E_s)]}M_{i,L'}^*\right)\,, \qquad (4)$$

where the collective angular momentum index $L=(l,m)$, $k=(2mE_s)^{1/2}/\hbar$ is the wave vector of the photoelectron, $\tau^{00}_{LL'}$ are matrix elements of the scattering path operator τ which sums all paths that begin and end at the site of the excited atom in angular momentum states L and L', respectively, the matrix elements $M_{i,L}$ are given by

$$M_{i,L}=\int d\mathbf{r}\,\psi_i^*(\mathbf{r})e^{i\mathbf{q}\cdot\mathbf{r}}\psi_L(\mathbf{r}) \tag{5}$$

with $\psi_i(\mathbf{r})=R_{l_i}(r;E_i)Y_{L_i}(\hat{\mathbf{r}})$, $\psi_L(\mathbf{r})=R_l(r;E_s)Y_L(\hat{\mathbf{r}})$, and $R_l(r;E_s)$ is the regular solution at energy E_s of the radial Schrödinger equation for the muffin-tin potential of the excited atom. In spherical coordinates, $\mathbf{r}=(r,\theta,\phi)$, so that $\hat{\mathbf{r}}=(\theta,\phi)$. Finally, $t_l^0(E_s)$ is the reflection coefficient of the Lth partial wave at energy E_s given in terms of the phase shifts $\delta_l(E_s)$ by

$$t_l^0(E_s)=\tfrac{1}{2}\left(e^{2i\delta_l(E_s)}-1\right). \tag{6}$$

In terms of the transition rate per unit time W, the differential cross section, i.e., the transition rate per unit time per unit energy is given by

$$\frac{\partial\sigma^2}{\partial\Omega_f\,\partial E}d\Omega_f=\frac{W}{j_{\rm inc}}dv_f\propto W\frac{k_f}{k_{\rm inc}}d\Omega_f\,, \tag{7}$$

where Ω_f is the solid angle of $\mathbf{k}_f$, $j_{\rm inc}$ is the current density of the primary beam, and dv_f is the differential phase-space element around $\mathbf{k}_f$.

In almost every case, the primary electron undergoes elastic backscattering (either before or after inelastic scattering) to emerge from the solid, so we consider one inelastic event and one or more elastic events. Thus, we have incident primary electrons from every direction with respect to the site of the inelastic event, so the directions $\mathbf{k}_{\rm inc}$ and $\mathbf{k}_f$ are not fixed. We must therefore integrate over all incident directions or, because scattering depends only upon the momentum transfer, over all possible directions of $\mathbf{q}$. Since

$$q^2=k_{\rm inc}^2+k_f^2-2k_{\rm inc}k_f\cos\theta_{{\rm inc},f} \tag{8}$$

and

$$q\,dq=k_{\rm inc}k_f\sin\theta_{{\rm inc},f}\,d\theta_{{\rm inc},f}\,, \tag{9}$$

where $\theta_{{\rm inc},f}$ is the angle between $\mathbf{k}_{\rm inc}$ and $\mathbf{k}_f$, then using (9) and the fact that $d\Omega_f=\sin\theta_{{\rm inc},f}\,d\phi_{\rm inc}\,d\theta_{{\rm inc},f}$, (7) becomes

$$\frac{\partial\sigma^2}{\partial q\,\partial E}dq\propto\int\int_0^{2\pi}d\phi_{\rm inc}\,W\frac{q\,dq}{k_{\rm inc}^2}\propto\int\int_0^{2\pi}d\phi_{\rm inc}\,W q\,dq\,. \tag{10}$$

Note from (4) and (5) that $W=W(\mathbf{q})$ depends on the orientation of $\mathbf{q}$ with respect to the sample, and that for given directions $\mathbf{k}_{\rm inc}$ and $\mathbf{k}_f$ of the primary beam in an angle-resolved experiment, $\hat{q}$ and q change with the energy loss $\Delta E=E_{\rm inc}-E_f$. However, for a narrow energy range (in the near-edge region), ΔE may be considered to be constant.

From (4) and (10) we see that the differential cross section is proportional to q^{-3}. Thus, $q_{\rm min}$, the minimum momentum transfer for a given energy loss, gives the most important contribution, and the quantity to compare with experiment is

$$\int d\Omega_{\rm inc}\frac{\partial\sigma^2}{\partial q\,\partial E}\propto\int W q\,d\Omega_{\rm inc}=\int W q\,d\Omega_q\,, \tag{11}$$

where $d\Omega_q$ is the solid angle of $\mathbf{q}$.

The quantities needed for the calculation are $\tau^{00}_{LL'}$, $R_l(r;E_s)$, $M_{i,L}$, and the phase shifts of the lth partial wave at energy E_s, $\delta_l(E_s)$. Phase shifts, wave functions,

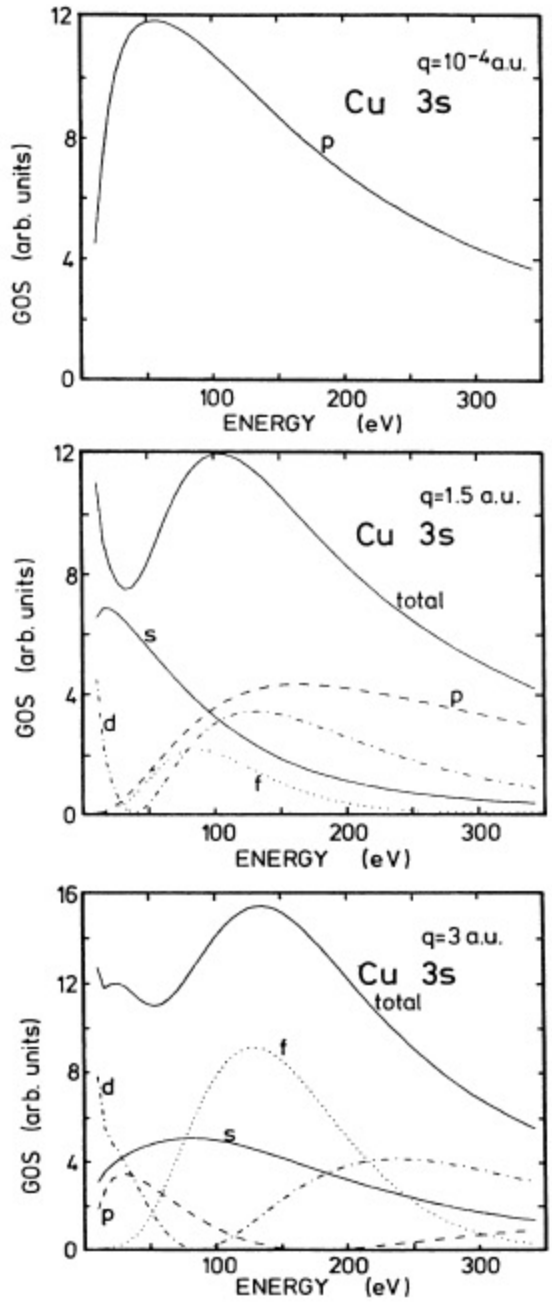

FIG. 1. Generalized oscillator strength as a function of energy, E_s, for $3s$ excitations in copper. Plots labeled s, p, d, and f show contributions to different final-state symmetries summed up to the total GOS at three different momentum transfers q. The top panel represents the dipole case.

and matrix elements are produced with a program that solves the Schrödinger equation for a muffin-tin potential. Phase shifts and matrix elements are then used as input to a modified version of ICXANES (Ref. 6) to calculate the elements of the τ matrix.

We first calculate the quantity $(\Delta E/q^2)|M_{i,L}(\mathbf{q})|^2$, which is proportional to the GOS. Figure 1 shows the GOS for the ionization of a Cu $3s$ core level for final states of $l=0,1,2,3$ for $q=10^{-4}$, 1.5, and 3.0 a.u. [q(a.u.) $=\sqrt{2E(\text{hartree})}=0.529q(\text{Å}^{-1})$, 1 hartree $=27.2$ eV]. The momentum transfer $\mathbf{q}$ is fixed in the z direction. We have chosen the $3s$ edge because the delocalized scattering picture is appropriate, as well as the necessity of integrating over a range of q to achieve agreement with experiment. For the $2p$ edge, the integration over q has almost no effect upon the primary features in the near-edge structure, while for the $3p$ edge, other electronic effects (e.g., relaxation) disturb the simple scattering picture.[10]

Figure 1 shows that dipole-allowed transitions are strongest for small q, but that dipole-forbidden transitions can be of the same strength or greater for larger values of q. In fact, only for small q is the GOS dominated by the $3s$-to-p transition, with dipole-forbidden transitions becoming increasingly dominant for $q=1.5$ a.u. and $q=3.0$ a.u. Note also the presense of the characteristic minimum for transitions to $l=2$ final states. To understand this, we begin with (5), invoke

$$e^{i\mathbf{q}\cdot\mathbf{r}}=4\pi\sum_{l=0}^{\infty}\sum_{m=-l}^{l}j_l(qr)Y_{l,-m}(\hat{\mathbf{r}})Y_{l,m}(\hat{\mathbf{q}})\,, \tag{12}$$

to obtain for the matrix elements $M_{i,L'}$ the expression

$$M_{i,L'}=4\pi\sum_{l=0}^{\infty}\int_0^{\infty}dr\,R_{l_i}^{*}(r)j_l(qr)R_{l'}(r)\sum_{m=-l}^{l}(-1)^{m+m_i}Y_L(\hat{\mathbf{q}})\int d\Omega\,Y_{l_i,-m_i}(\hat{\mathbf{r}})Y_{l,-m}(\hat{\mathbf{r}})Y_{l',m'}(\hat{\mathbf{r}})\,. \tag{13}$$

Thus, the minimum for d final states is due to the extinction of the radial integral when the nodes of the Bessel function with q and those of the final-state wave function with E_s move through the overlap region of the core wave function.

The comparison between measured and calculated energy-loss structure near the Cu $3s$ edge is shown in Fig. 2, including a comparison with a calculation based upon the dipole approximation, i.e., where the exponential in the matrix element is expanded as

$$e^{i\mathbf{q}\cdot\mathbf{r}}\approx 1+i\mathbf{q}\cdot\mathbf{r}\,. \tag{14}$$

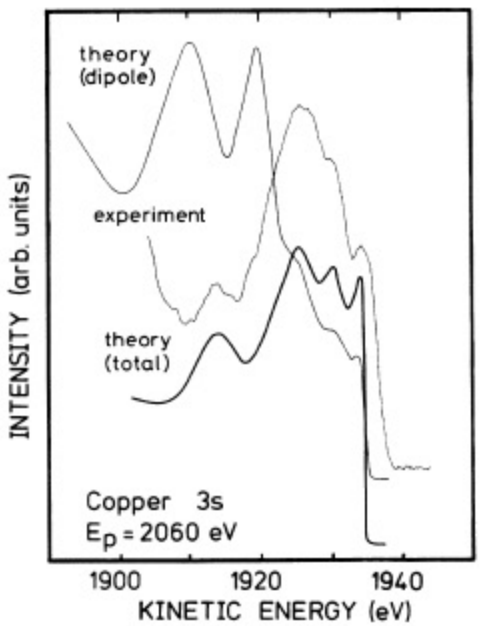

FIG. 2. Electron-energy-loss spectrum obtained from Cu(001) around loss energies of 120–160 eV, representing the $3s$ excitation, compared with theoretical cross sections calculated with the dipole approximation (14), labeled theory (dipole), and with contributions from all angular momenta, labeled theory (total).

Primary electrons of 2060 eV were used, and a cubic spline has been subtracted to eliminate the background of secondary electrons. A cluster representative of the bulk produced better agreement with experiment than calculations using clusters representative of the Cu(001) surface, indicating that a substantial part of the information originates at least from the second layer. The total cross section was calculated by integrating from $q_{\min}=0.36$ a.u. to $q=6$ a.u. and over $d\Omega_q$. Note first that there are discrepancies between the calculation based upon the dipole approximation and the measured spectrum in both the relative intensities *and* positions of the peaks. However, the common features between measured and calculated spectra based upon the actual matrix element (5) are in excellent agreement with regard to relative energy positions, though the measured relative intensities are not as well reproduced. This could be due to contributions from other edges ($3p$,$3d$) in this region. The central point, however, is that because the energy profile GOS is strongly energy dependent (Fig. 1), and shows pronounced contributions from dipole-forbidden transitions, an integration over the absolute value of the momentum transfer for the computation of the cross section is crucial for meaningful comparisons between measured and calculated spectra. In a separate publication[10] we will provide similar comparisons near other Cu edges to place the results obtained here into a wider context.

One of us (D.D.V.) acknowledges the hospitality of Eidgenössische Technische Hochschule–Zürich during his visits. This work is partly supported by the Schweizerischer Nationalfonds zur Förderung der wissenschaftlichen Forschung. Computer time on the Cray Research, Inc. X-MP/28 computer provided by the Eidgenössische Technische Hochschule Rechenzentrum is gratefully acknowledged.

*Present address: Institute for Materials Research, McMaster University, Hamilton, Ontario, Canada L8S 4M1.

†Present address: Department of Materials Science and Engineering, Stevens Institute of Technology, Hoboken, NJ 07030.

‡Permanent address: The Blackett Laboratory, Imperial College of Science, Technology and Medicine, University of London, London SW7 2BZ, United Kingdom.

[1] *EXAFS Spectroscopy: Techniques and Applications,* edited by B. K. Teo and D. Joy (Plenum, New York, 1981).

[2] M. de Crescenzi and G. Chiarello, J. Phys. C **18**, 3595 (1985).

[3] L. Hedin and B. I. Lundqvist, J. Phys. C **4**, 2064 (1971).

[4] *Giant Resonances in Atoms, Molecules, and Solids,* edited by J. P. Connerade, J. M. Esteva, and R. C. Karnatak (Plenum, New York, 1987).

[5] P. J. Durham, J. B. Pendry, and C. H. Hodges, Comput. Phys. Commun. **25**, 193 (1982).

[6] D. D. Vvedensky, D. K. Saldin, and J. B. Pendry, Comput. Phys. Commun. **40**, 421 (1986).

[7] A. Šimunek, O. Šipr, and J. Vackář, Phys. Rev. Lett. **63**, 2076 (1989).

[8] A. Šimunek, J. Vackář, and E. Sobczak, Phys. Rev. B **38**, 8515 (1988).

[9] D. K. Saldin, Philos. Mag. B **56**, 515 (1987).

[10] P. Aebi, M. Erbudak, F. Vanini, D. D. Vvedensky, and G. Kostorz, Phys. Rev. B **41**, 11 760 (1990).

[11] D. K. Saldin, Phys. Rev. Lett. **60**, 1197 (1988).

[12] V. I. Ochkur, Zh. Eksp. Theor. Fiz. **45**, 734 (1963); **47**, 1746 (1964) [Sov. Phys. JETP **18**, 503 (1964)]; **20**, 1175 (1965)].